

WFC3 Instrument Science Report 2009-02

WFC3 TV3 Testing: Orbital Cycling Effects on IR Images

H. Bushouse
March 26, 2009

ABSTRACT

Orbital cycling tests were performed on WFC3 during Thermal-Vacuum test #3 in order to assess the impact of changing thermal and electrical environments on the stability of the IR detector. Variations in IR dark current resulting from the changing environments during orbital cycling appear to be relatively small, amounting to a total difference in accumulated dark signal of ~ 18 e/pixel over a 6-minute exposure. The variation in dark current appears to occur as a uniform shift in the dark rate per pixel. The raw zeroth-read signals are mildly correlated with WFC3 input voltage, but the effect is complicated by an unexpected systematic variation in the reset level from exposure to exposure that appears to be dependent on exposure history. The changes in bias level track well across all image quadrants and the amplitude of the drifts is significantly reduced, but not completely eliminated, by the calibration process. There is no indication of the type of quadrant-to-quadrant bias residuals seen in NICMOS images.

Introduction

During WFC3 thermal-vacuum test #3 (TV3) at Goddard Space Flight Center, tests were performed that simulated the cyclical changes in both thermal and electrical environments that WFC3 will experience as it orbits the Earth in HST. The primary purpose of these tests was to examine the ability of the WFC3 IR detector cooling systems to maintain a stable Focal Plane Array (FPA) temperature in the face of varying thermal loads and electrical input from the HST power bus, which are caused by

repeatedly traversing orbital day and night conditions. The voltage level of the power being received from HST goes from a peak of ~ 32 V when the sun is illuminating the solar arrays and the spacecraft batteries are fully charged, to a minimum of ~ 26 V as HST approaches the end of orbital night and the batteries reach their minimum charge levels. If the WFC3 IR detector cooling systems allow the FPA temperature to vary under these conditions, the changes in the FPA temperature would in turn lead to changes in the rate of dark current accumulation during IR exposures, making it difficult to obtain accurate calibrations of the exposures.

Analysis of the behavior of the NICMOS detectors under similar conditions has shown that these types of changes in environment can also lead to changes in other detector properties, such as the reset level (Bergeron 2005), which then leads to yet more complications in the calibration process. Thus a second goal of these TV3 tests was to look for any similar behaviors in the WFC3 IR flight detector. Note that in our subsequent discussions of these types of tests we will use the term “bias” to refer to the signal recorded in the “zeroth” readout of an IR exposure, which occurs immediately after the detector pixels have been reset. Although it is not a true bias signal, as in the case of CCD detectors, it is treated similarly, in that it is an instrumental signal that must be subtracted from the raw detector signal in order to recover the accumulation of real signal that takes place during the exposure.

Test Details

The orbital cycling tests were performed three times during TV3. The first two episodes were executed on March 5 and 6, 2008, respectively, with WFC3 in a cold orbital environment. The test on March 5 was done with WFC3 running on its Side 2 (MEB2) electronics, while the March 6 test was performed on Side 1 (MEB1). The third episode occurred on March 20, 2008, with WFC3 in a hot orbital environment and operating on the Side 1 electronics. This last test is the most challenging of the three, because the hot environment produces the largest load on the IR detector cooling systems, as well as the largest orbital temperature variations.

During each of the three test episodes, the thermal environment presented to the WFC3 radiator was cycled to match model predictions of what it will experience on orbit. At the same time, a WFC3 operations command script was executed to vary the voltage level of the power being fed to WFC3 from the power distribution unit (PDU) used during ground tests. The variations in voltage level were synchronized with the thermal changes in order to mimic the expected on-orbit conditions as closely as possible, using an orbital period of ~ 96 minutes. The input voltage curve was in fact copied from actual readings taken from other science instruments on HST. Each test episode lasted for a total of about 5 hours, allowing for three full orbital cycles to be executed.

While the orbital cycles were being executed, WFC3 was commanded to take a continuous set of IR dark exposures, using ground test Science Mission Specification

(SMS) IR24S02. Dark exposures use the blank position of the IR Filter Select Mechanism (FSM) to block out all incoming light. The IR24S02 SMS takes a series of IR full-frame darks using the SPARS25 readout sequence (SAMP_SEQ) and the maximum of 15 readouts, resulting in a total duration of 353 seconds for each IR exposure. This exposure time is long enough to allow for parallel dumping of the data from each exposure while the next exposure is executing. During the first test, images were obtained during only the first ~ 1.5 orbital cycles, while a full 3 cycles were covered in the second and third tests. The images obtained during each of the three test episodes are listed in Tables 1-3 in the appendix. The tables list the WFC3 ground test image database number (TVNUM), the OPUS root file name, the start date/time of the exposure (TVSTART), the voltage level of the PDU at the start of the exposure, and the IR FPA temperature as recorded in the IRFPATMP keyword in the `_spt.fits` file headers.

The focus of this report is not on the achieved FPA temperature stability during the cycling tests. Those results are relevant, however, because changes in FPA temperature will in turn affect the detector dark current. The FPA temperature telemetry readings from cycling test 3 are shown in Figure 1. Notice that the resolution of the telemetry calibration curve results in differences of $\sim 0.09^\circ\text{C}$ for each “tick” up or down in the raw telemetry value. For most of test 3, the temperature values oscillated between -128.80 and -128.71 , with a few excursions up to -128.62 . The few excursions to higher temperature generally occurred near the times when the WFC3 input voltage was the lowest. A smoothed fit to the temperature values (D. Rossetti, private communication) is shown in Figure 2, which confirms that the FPA temperature is in fact inversely correlated with the WFC3 power level, resulting in peak-to-peak changes in temperature of $\sim 0.06^\circ\text{C}$ over a single orbit cycle.

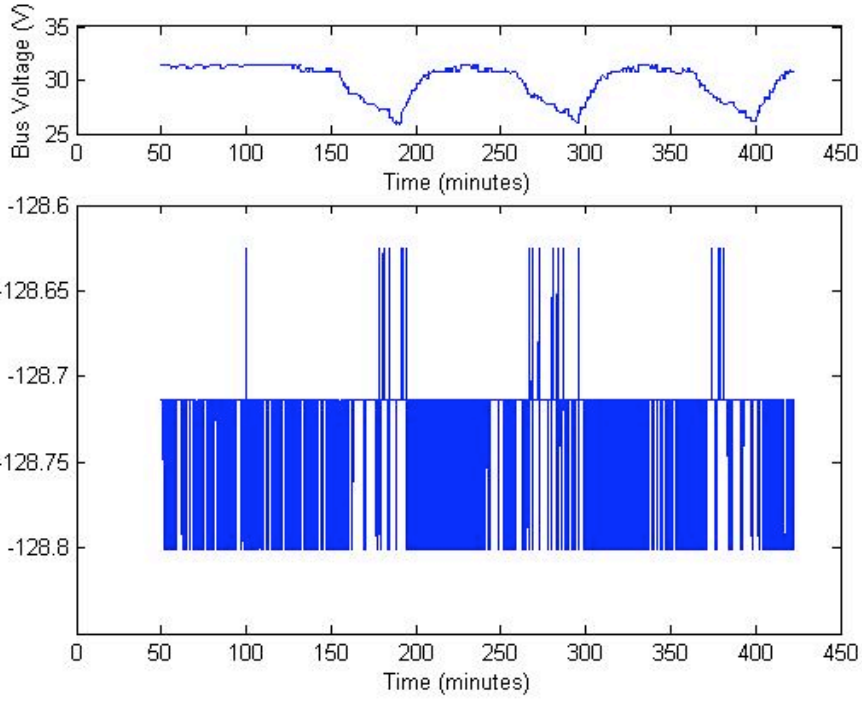


Figure 1. FPA temperature telemetry values during orbital cycling test 3.

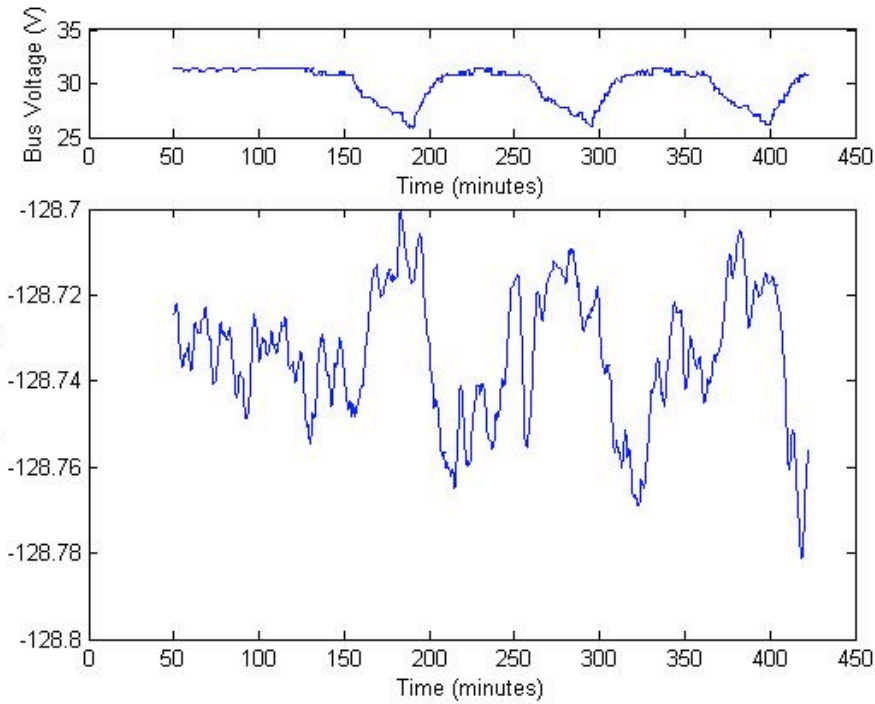


Figure 2. Interpolated FPA temperature values during orbital cycling test 3.

Dark Current vs. Orbital Cycling

All of the IR dark exposures were processed through the OPUS pipeline, producing `_raw.fits` files. The raw files were then processed with `calwf3 v1.1`, which included reference pixel bias level corrections for each readout (BLEVCORR) and subtraction of the zeroth read from each subsequent readout in an exposure (ZOFFCORR). The current reference pixel correction scheme takes the sigma-clipped mean of all vertical reference pixels (i.e. those located at the left and right edges of an image) for each readout and subtracts that mean value from the imaging area pixels in that readout.

The resulting `_ima.fits` files produced by `calwf3` were analysed to measure the dark current rate in each exposure. This was done by first using the STSDAS task “`pstats`” to compute the mean signal value in each readout of a given exposure, with a sigma-clipping procedure employed to reject hot pixels and other outliers. The stack of readout time vs. signal for each exposure was then fitted with a linear function using the STSDAS task “`gfit1d`”, where the slope of the fit then gave the dark current rate in units of DN/sec. The first readout of each exposure was not used in the fit, because it appears to suffer from reset non-linearity effects. The resulting dark rates were converted to electrons per second using an adopted gain of $2.26 \text{ e}^-/\text{DN}$ for the IR-4 detector (Hilbert 2008). Plots showing the IR dark current vs. PDU voltage cycling are shown in Figures 3 through 5 for each of the three test episodes.

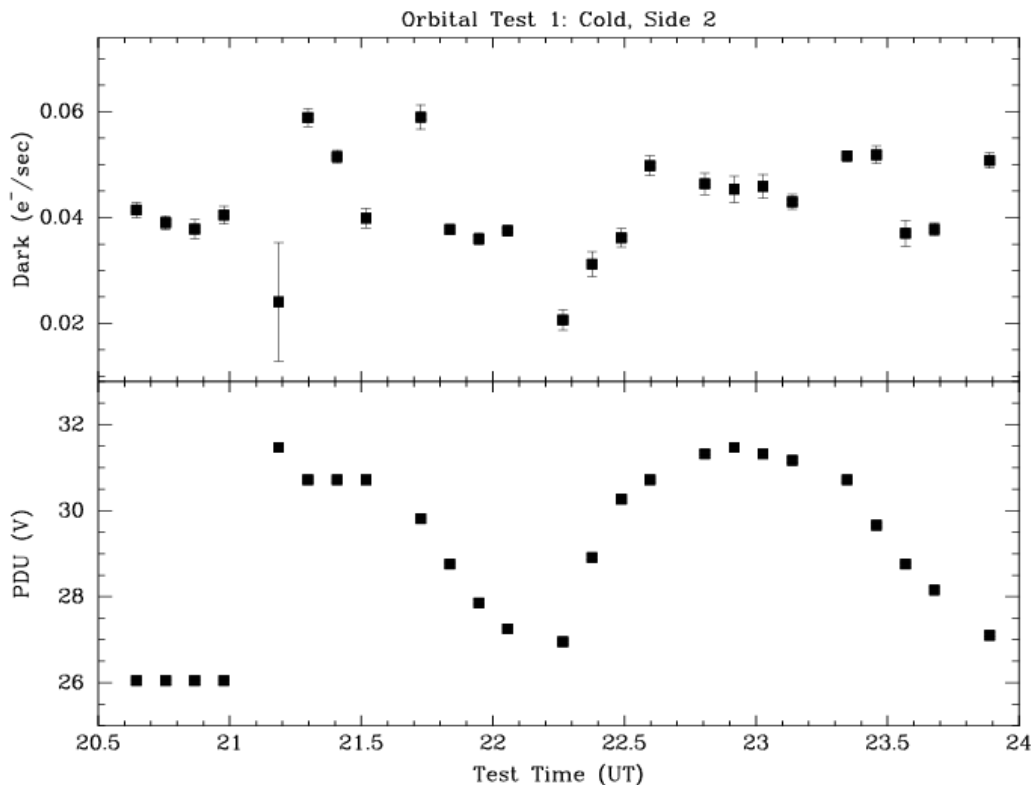


Figure 3. Dark current and PDU voltage for each exposure during orbital cycling test 1.

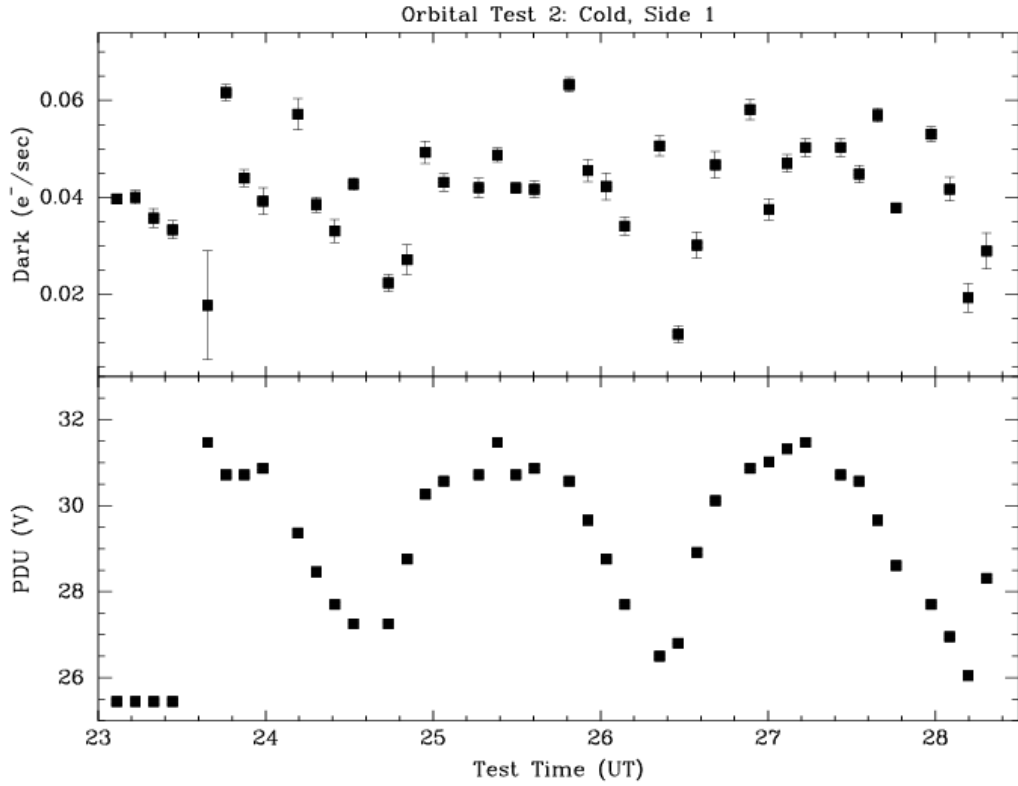


Figure 4. Dark current and PDU voltage for each exposure during orbital cycling test 2.

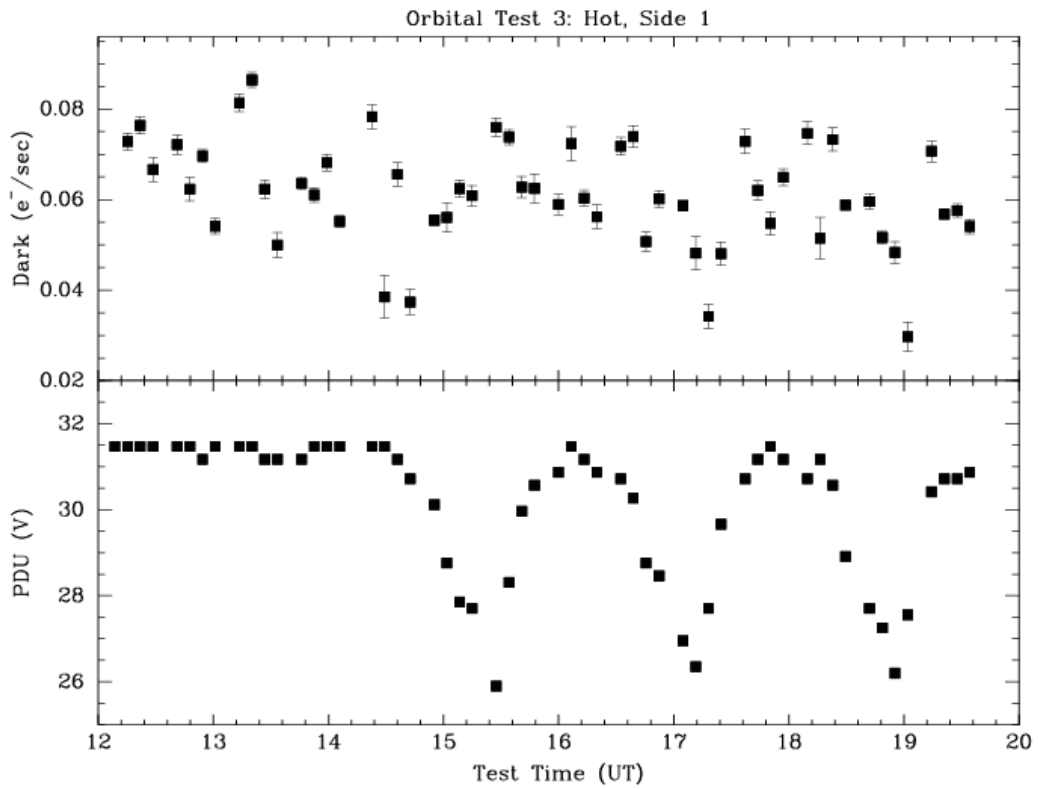


Figure 5. Dark current and PDU voltage for each exposure during orbital cycling test 3.

The plots show how the PDU voltage was initially held constant for some amount of time at the beginning of each test, in order to establish a baseline of dark current behavior. In tests 1 and 2, the PDU voltage was held at ~ 26 V for the first 4 exposures, after which it was raised to ~ 31.5 V for the start of the cycling procedure. This unrealistically sudden change in voltage produced large non-linearities in the IR detector behavior for the exposure that was in progress at that time. During the third test, a more sensible strategy was used, in which the PDU voltage was held constant at ~ 31.5 V for the first 16 exposures – during which the thermal environment was cycling – and then the voltage cycling procedure was started, with no sudden jump in voltage either during or between exposures.

Overall, the IR FPA dark current appears to be relatively insensitive to the effects of the orbital cycling. The lowest dark current readings do seem to preferentially occur at or near the minima in the voltage curves, but there are also times when the dark current level is normal or even a bit higher than normal at the time of a voltage minimum. Note too how much the dark current readings vary during the initial phase of test 3, when the PDU voltage was constant. These variations could be due to the thermal cycling that was already underway at that time.

Figures 6 through 8 show the dark current measurements plotted directly against PDU voltage for the three tests. The results of linear least-squares fits to the data are shown as dotted lines in each plot. The fits consistently indicate a change in dark current of ~ 0.0023 $e^-/\text{sec}/\text{V}$, thus confirming the impression that the dark current tends to be somewhat lower, on average, for lower values of PDU voltage. Note, however, that there is a large amount of scatter about this fit for individual exposures. For two exposures taken at the extremes of the PDU voltage range, the total difference in accumulated dark over the course of the 353 second exposures used in this test would amount to ~ 5 e^-/pix . If a mean dark current reference image were subtracted from such a science exposure during calibration, the maximum residual error in dark current subtraction would be half that level. On a per pixel basis this would be less than the typical read noise. Averaged over a large source, however, it could become significant.

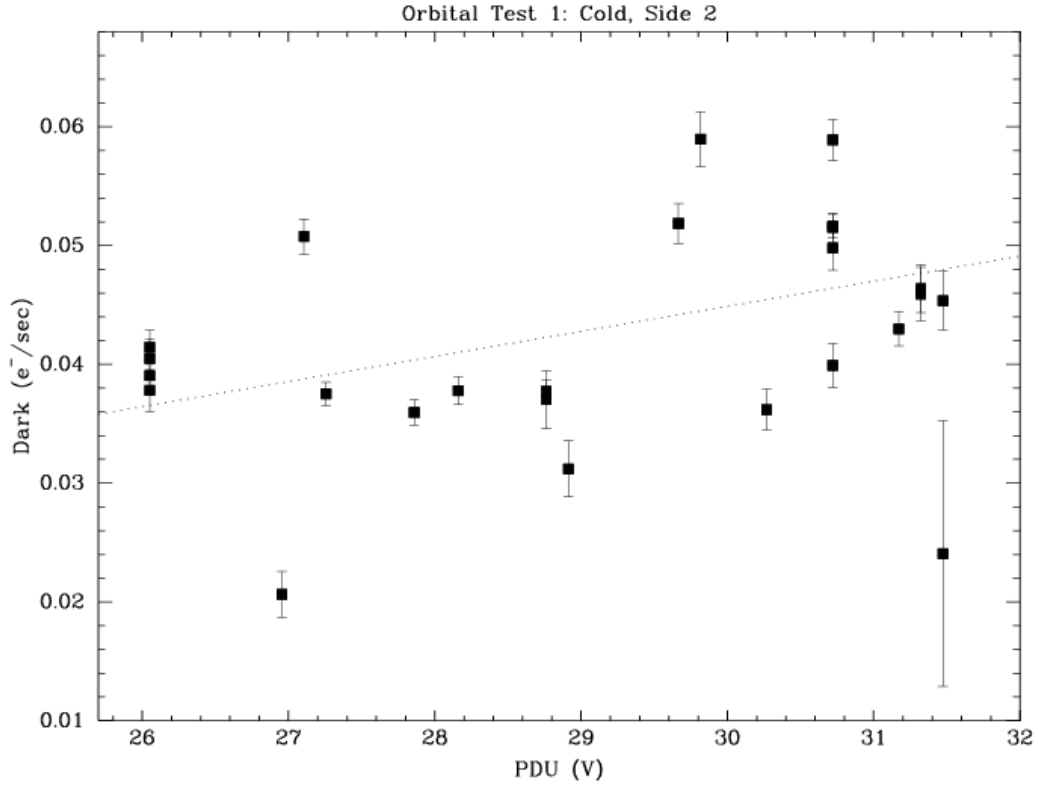


Figure 6. Dark current vs. PDU voltage for orbital cycling test 1.

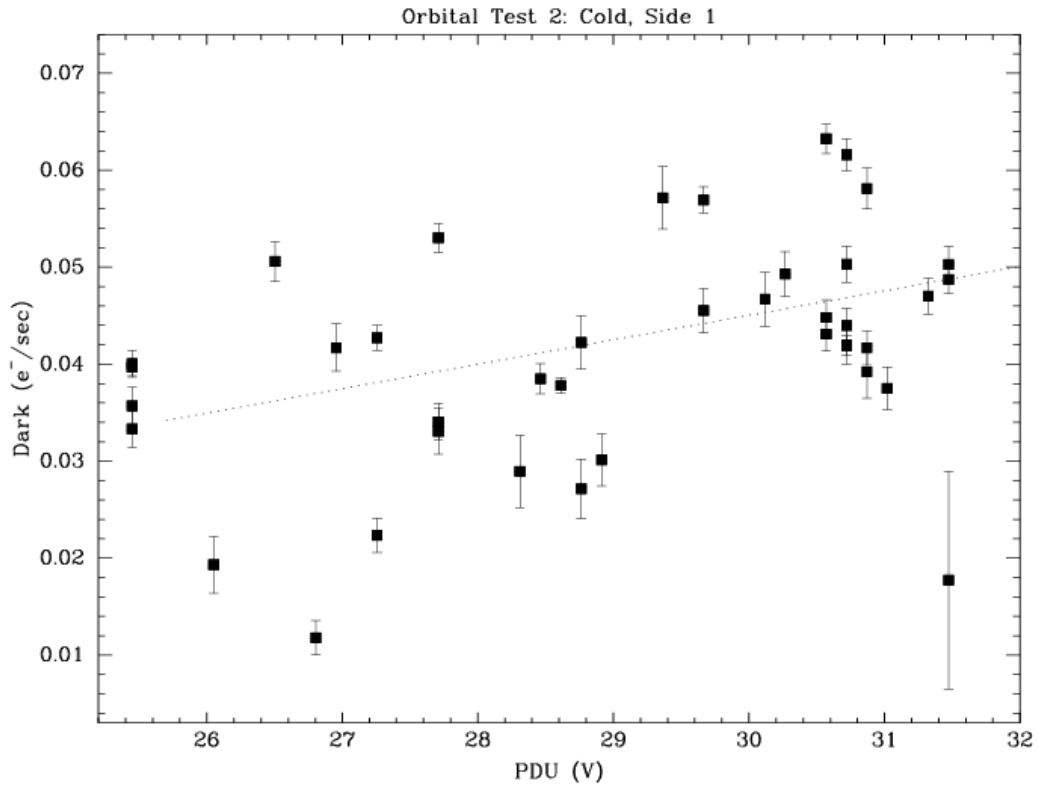


Figure 7. Dark current vs. PDU voltage for orbital cycling test 2.

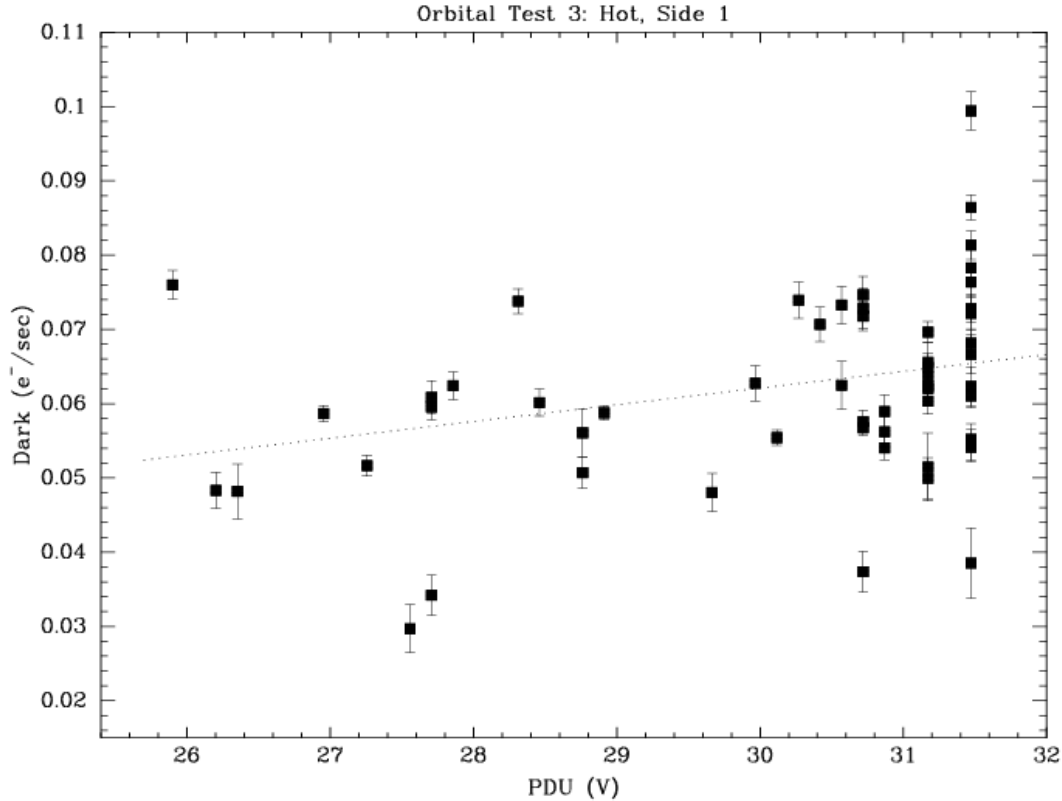


Figure 8. Dark current vs. PDU voltage for orbital cycling test 3.

The way in which the dark current is varying is also of interest. For example, is it increasing uniformly from pixel-to-pixel or are the variations perhaps correlated with the nominal dark rate of each pixel such that pixels with higher nominal rates show larger increases? We have investigated this using several different types of analysis.

First, we have compared the dark current histograms for images with the lowest rates against those with the highest. One such pair of low vs. high rate images is images 52779 and 52780 within the test 3 sequence, which were taken right about the time of the last voltage minimum at ~ 19 UT in test 3 (see Figure 5 and Table 3). Image 52779 has a dark rate of ~ 0.03 e^-/sec , while image 52780 is ~ 0.07 e^-/sec . Figure 9 shows the superimposed histograms of these two images. This clearly shows that the difference between the two amounts to a simple shift of the entire distributions of dark rates per pixel, with no indication of any change in the population of high dark current pixels. The widths of the peaks of the two histograms are also essentially identical.

Another way to look at this is to take the difference of the two images, pixel-by-pixel, and investigate the histogram of the resulting difference image. This is shown in Figure 10, where we see that there is no significant asymmetry to the histogram or any indication of a residual high dark current tail.

Finally, we have also done pixel-to-pixel comparisons of low vs. high dark rate images. Examples are shown in Figure 11 and Figure 12, this time using images 52766 and 52768 from test sequence 3, which occurred near the second minimum in PDU

voltage and have mean dark rates of 0.034 and 0.073 e^-/sec , respectively. Figure 11 shows a wide range of dark rates up to a maximum of 6 e^-/sec , while Figure 12 shows a more restricted subset up to 0.6 e^-/sec . The dotted line in each figure is simply a 45° diagonal with a vertical offset equal to the difference in mean dark rates for the two images. The figures show that there is a very good correlation between the dark rates of specific pixels in the two images.

All of these results indicate that the change in dark current due to orbital cycling occurs as a uniform shift in the mean dark current per pixel. There is no indication of any specific change in the behavior of or the fraction of pixels with higher than normal dark current.

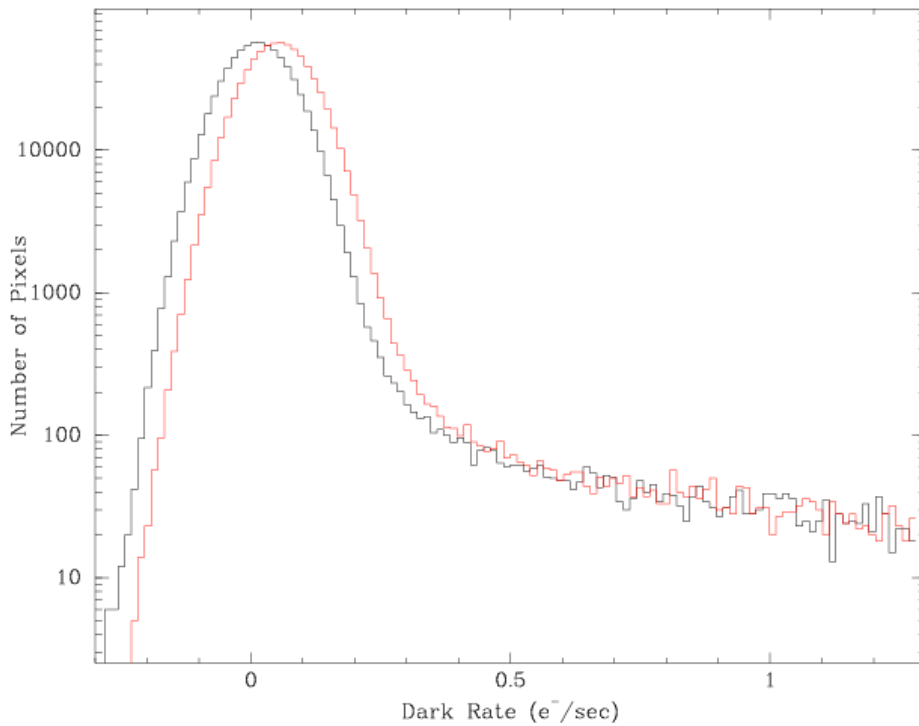


Figure 9. Histograms of the dark current per pixel in images 52779 (black line) and 52780 (red line) from test sequence 3.

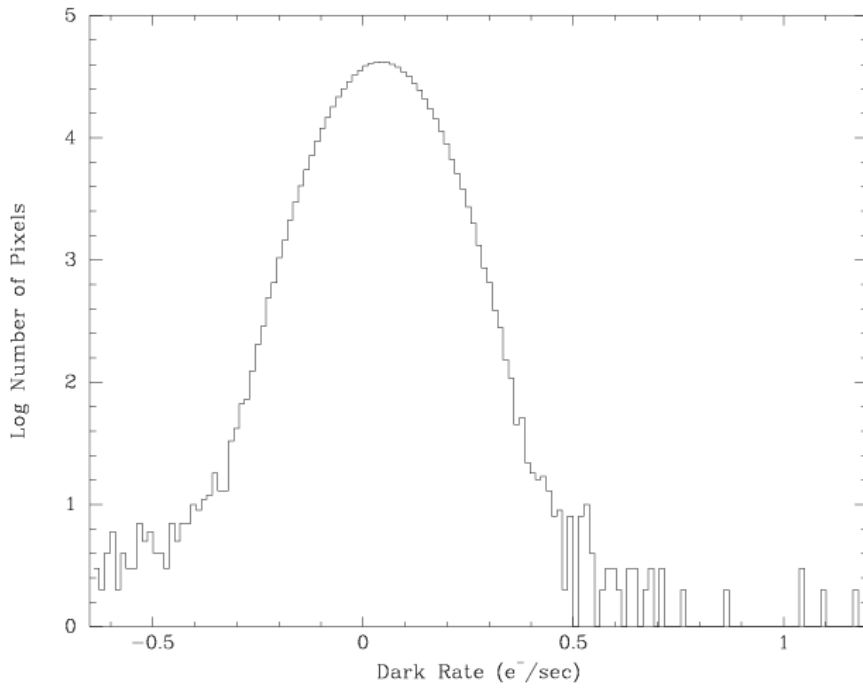


Figure 10. Histogram of the difference of images 52780 and 52779 from test sequence 3.

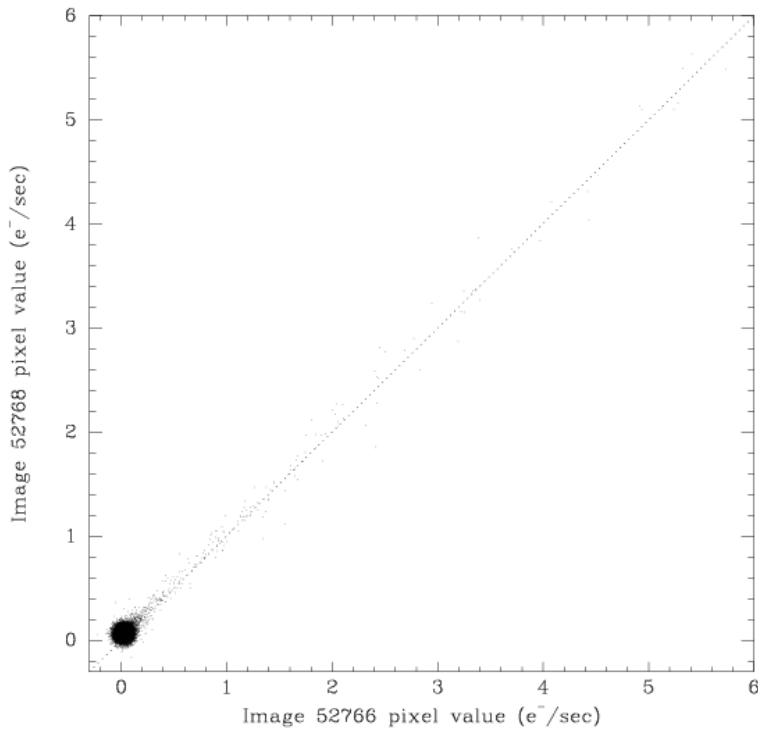


Figure 11. Pixel-vs-pixel plot of a subsection of images 52766 and 52768 from test sequence 3. The diagonal dotted line corresponds to perfect correlation with an offset equal to the difference in mean dark rate.

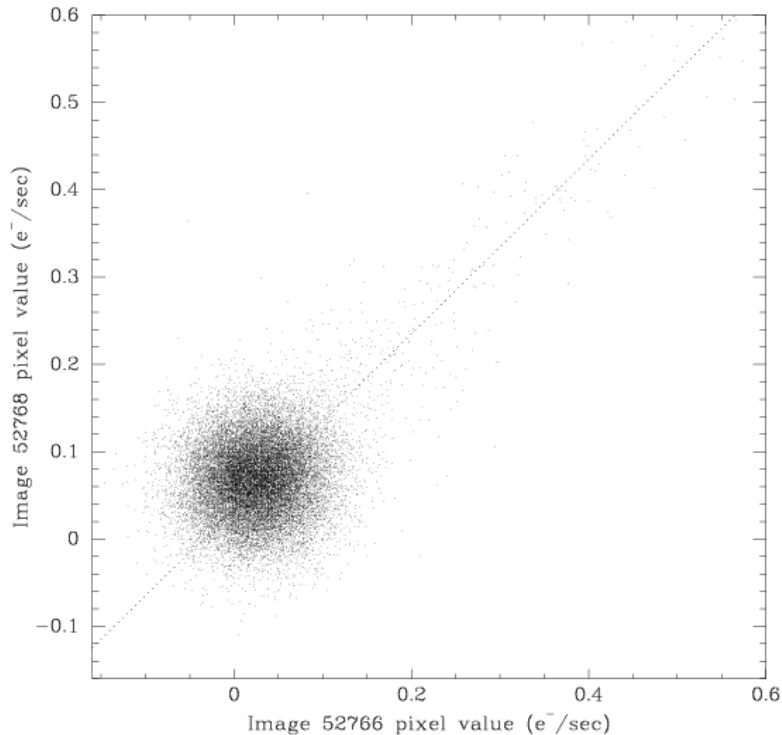


Figure 12. Pixel-to-pixel plot of a subsection of images 52766 and 52768 from test sequence 3. The diagonal dotted line corresponds to perfect correlation with an offset equal to the difference in mean dark rate.

Bias Stability vs. Orbital Cycling

Bergeron (2005) has shown that the bias levels of the NICMOS detectors varies with both FPA temperature and the NICMOS instrument input voltage level received from HST. Furthermore, due to the fact that the exact readout timing of each detector quadrant varies according to its phasing with the NICMOS low voltage power supply (LVPS), the variation in bias level from image to image is not the same for all detector quadrants. These two effects add severe complications to the NICMOS data calibration process.

The WFC3 TV3 orbital cycling data sets were examined for any similar effects. First, the raw bias level in the zeroth read of each IR dark exposure was measured to look for trends as a function of the WFC3 PDU voltage level. Figures 13-15 show the mean bias levels (as measured from the zeroth read) in quadrants 1 and 4 for each of three orbital test episodes. These plots suggest a weak tendency for the zeroth read bias level to increase as PDU voltage decreases, but the correlation is complicated by an unexpected effect.

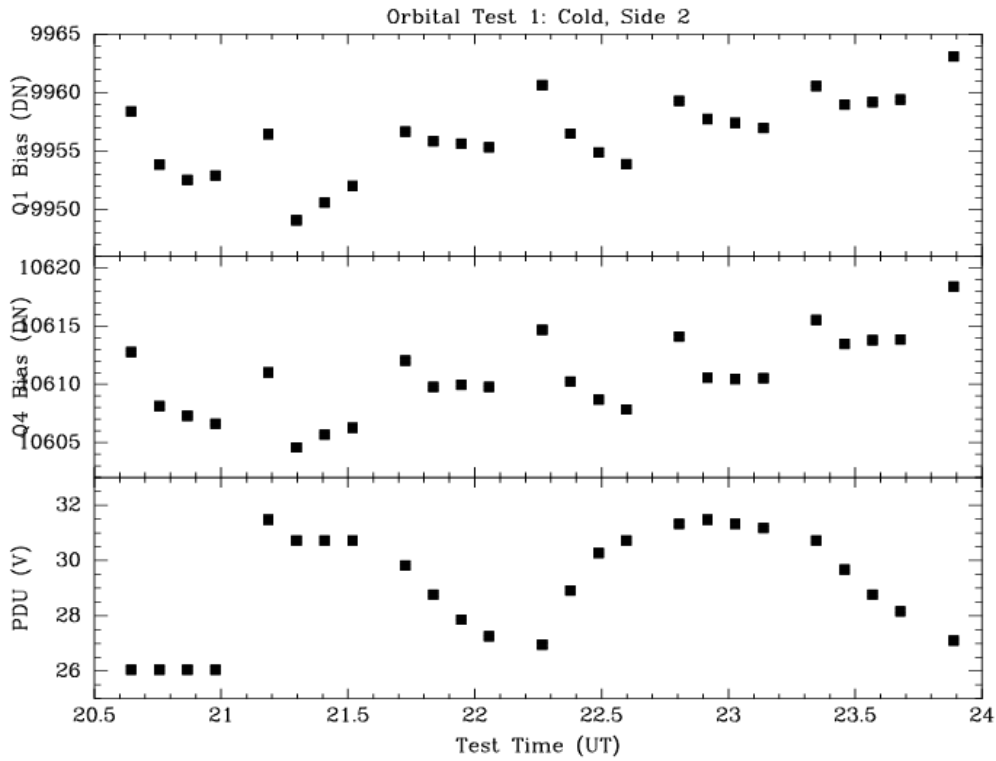


Figure 13. Mean zero-read bias levels in quadrants 1 and 4 for orbital cycling test 1.

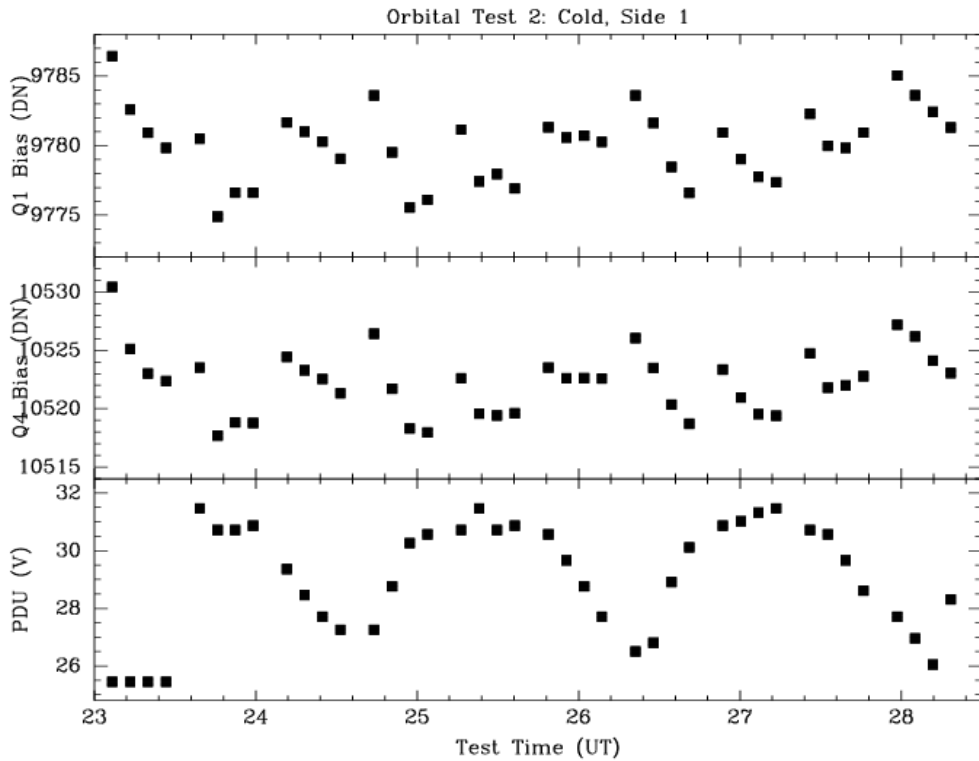


Figure 14. Mean zero-read bias levels in quadrants 1 and 4 for orbital cycling test 2.

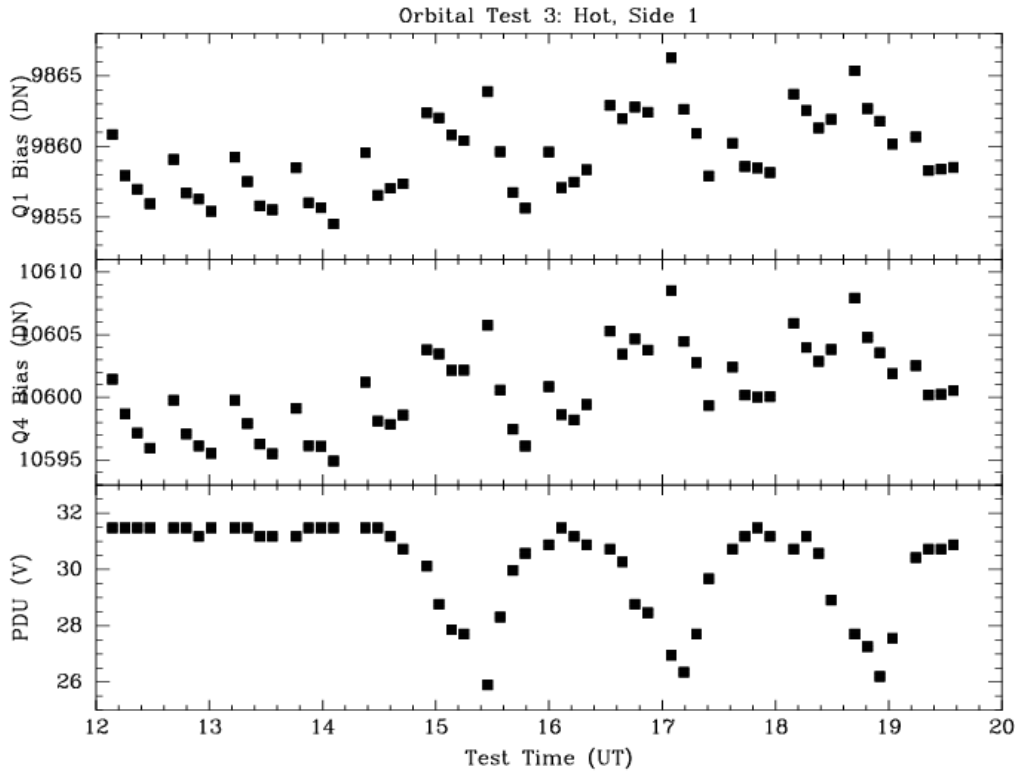


Figure 15. Mean zero-read bias levels in quadrants 1 and 4 for orbital cycling test 3.

The data from each dark exposure is usually dumped in parallel during the subsequent exposure, but due to the way that the IR24S01 SMS was built, a serial data dump occurred once every four exposures. The effect of this cadence in the dump process is evident in the zero-read bias levels: the first exposure in each set of four usually has a higher than normal bias level and then the bias level gradually decreases through the remaining 3 exposures. WFC3 and the IR detector then sit idle for 5.5 minutes after the fourth exposure, waiting for the serial dump to complete, after which the first exposure in the next set of four once again starts out at a higher bias level. This pattern repeats throughout the duration of each test.

In order to verify that this behavior is generic to WFC3 IR operations, rather than unique to the orbital cycling tests, we examined a series of IR dark exposures taken at another time during TV3, during which time the environment was stable and the instrument voltage was constant. Specifically, we looked at a series of 15 darks taken with SMS IR01S04 on March 19, 2008, performing the same measurements of the zeroth read mean bias level in quadrant 1 of each image. Figure 16 shows the results. For this test set, we see that the overall bias level was decreasing over the entire duration of the test, punctuated by the same periodic behavior that is associated with the data dumps. For this set of 15 exposures, serial dumps occurred after exposures 2, 6, 10, and 14. This results in exposures 1, 3, 7, 11, and 15 having unusually high bias levels, while the rest of

the exposures seem to follow the nominal trend. This confirms that the behavior is not unique to the darks taken during the orbital cycling tests. The cause of this behavior is not understood at this time and will be investigated further.

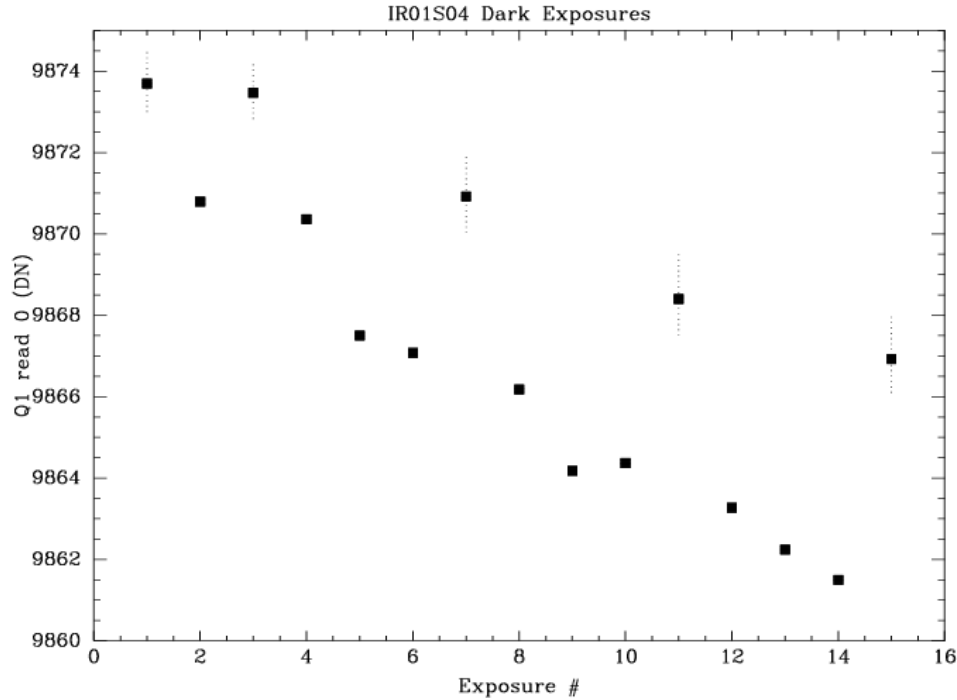


Figure 16. Quadrant 1 zeroth read bias for 15 darks from IR01S04 on March 19, 2008. Superimposed dotted lines indicate exposures taken immediately after a serial data dump.

Some additional investigations into the bias behavior of the orbital cycling exposures have been performed. Because cycling test 3 has the largest data set with which to work, we will concentrate on those data for the remainder of this report. First, the upper panels of Figures 13-15 indicate that the bias behavior appears to be nearly identical for quadrants 1 and 4. Other quadrants that are not shown behave the same way. Figure 17 confirms that there is in fact an excellent correlation between the bias signal in quadrants 1 and 4 for the exposures in test 3. The rms residuals from the fitted line are less than 0.5 DN. Thus the changes in bias from exposure to exposure track equally across the different image quadrants. Second, in order to determine if the changes in zero read bias track through to other readouts in the exposures, we measured the mean quadrant 1 signal in readout 3 and compared it to the signal in read 0. Readout 3 was chosen because it is past the point of being affected by reset anomalies at the beginning of each exposure, and yet it is still early enough in the exposure that it should not be affected in a significant way by the accumulation of dark current.

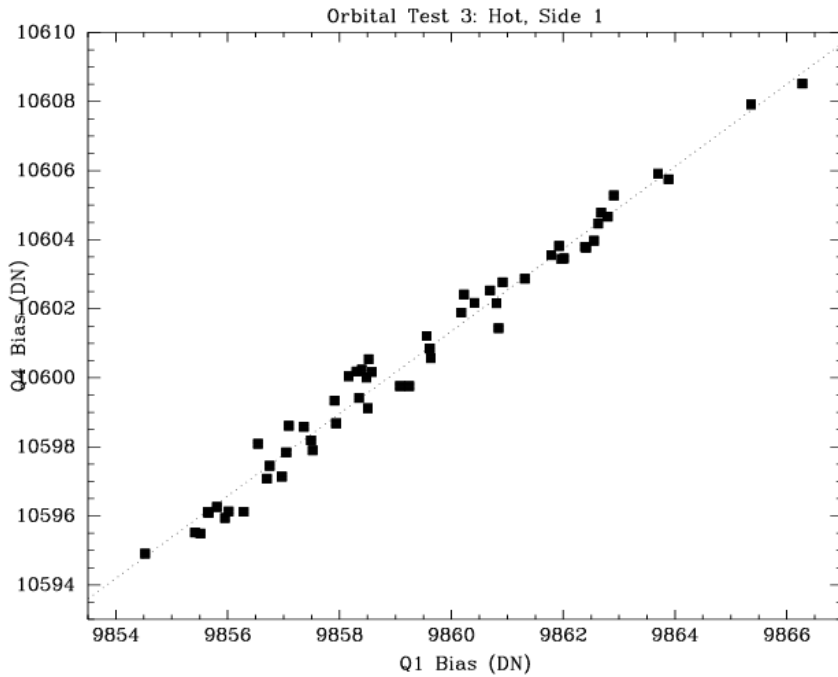


Figure 17. Quadrant 1 vs. quadrant 4 zero read bias levels for exposures in orbital cycling test 3.

The results are shown in Figure 18. Here the bottom panel shows the quadrant 1 raw signal in the zeroth read (bias) of each exposure and the middle panel shows the raw signal in the third read. There is a reasonably good correlation between the raw signal in the different readouts, indicating that the bias shifts from exposure to exposure are not just an artifact of the zeroth read, but track through to other readouts as well. We also measured the quadrant 1 signal in the third readout of the calibrated data files. The calibration process included bias drift corrections based on the reference pixel values in each readout and subtraction of the zeroth read from all subsequent reads. The calibrated quadrant 1 readout 3 values are shown in the top panel of Figure 18. The values indicate that the amplitude of the bias changes from exposure to exposure has been substantially decreased by the calibration process (range of ~ 15 DN in the raw images versus ~ 7 DN in the calibrated images), but is still present at a low level. Research into improved reference pixel corrections may be in order.

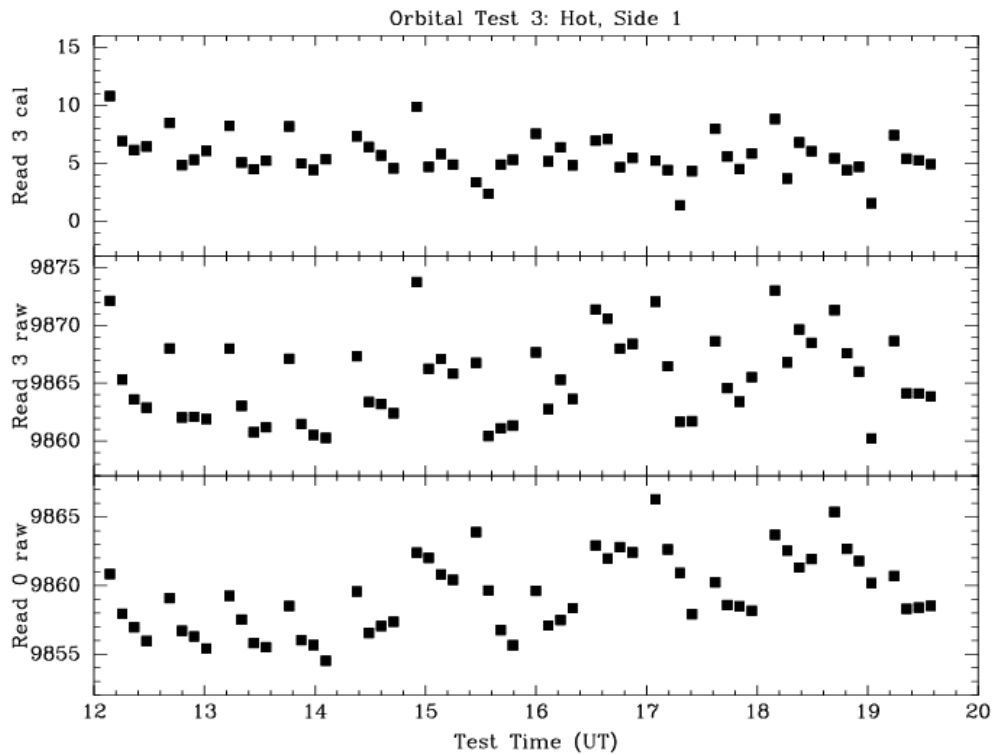


Figure 18. Quadrant 1 signal levels for the exposures in orbital cycling test 3. The bottom panel shows the raw signal in the zeroth read (bias level), the middle panel shows the raw signal in the third read, and the top panel shows the calibrated signal (after reference pixel correction and zero-read subtraction) in the third read.

A final look at bias behavior was done to see if the WFC3 IR images showed any of the same types of quadrant-to-quadrant drifts as NICMOS. We looked at this in two ways. First, we subtracted the raw zeroth read image of the first exposure in test 3 from the raw zeroth read of all other exposures in test 3. A sampling of 16 of those zero-read difference images is shown in Figure 19. There is no quadrant-to-quadrant structure in any of the difference images, indicating that the four image quadrants track one another well from exposure to exposure. This visual impression is supported by statistical analysis. Sigma-clipped means of the quadrants in each difference image show that residual offsets between quadrants are 1 DN or less. For example, Figure 20 shows the mean residuals for quadrant 3 vs. quadrant 4 along with a linear fit to the data. The fit coefficients indicate a systematic offset of only ~ 0.2 DN between these two quadrants, with an exposure-to-exposure scatter of ~ 0.25 DN.

Second, we subtracted the first entire exposure – readout by readout – from all subsequent exposures in test 3, resulting in a stack of 16 difference images for each exposure. A sampling of the results for 4 of the exposures is shown in Figure 21. As was the case when looking at only the differences of the zero reads, there are no obvious structural differences in the read-by-read subtractions of the full raw exposure sequences.

Thus WFC3 IR exposures should not encounter any quadrant-to-quadrant residuals during calibration, as is the case for NICMOS.

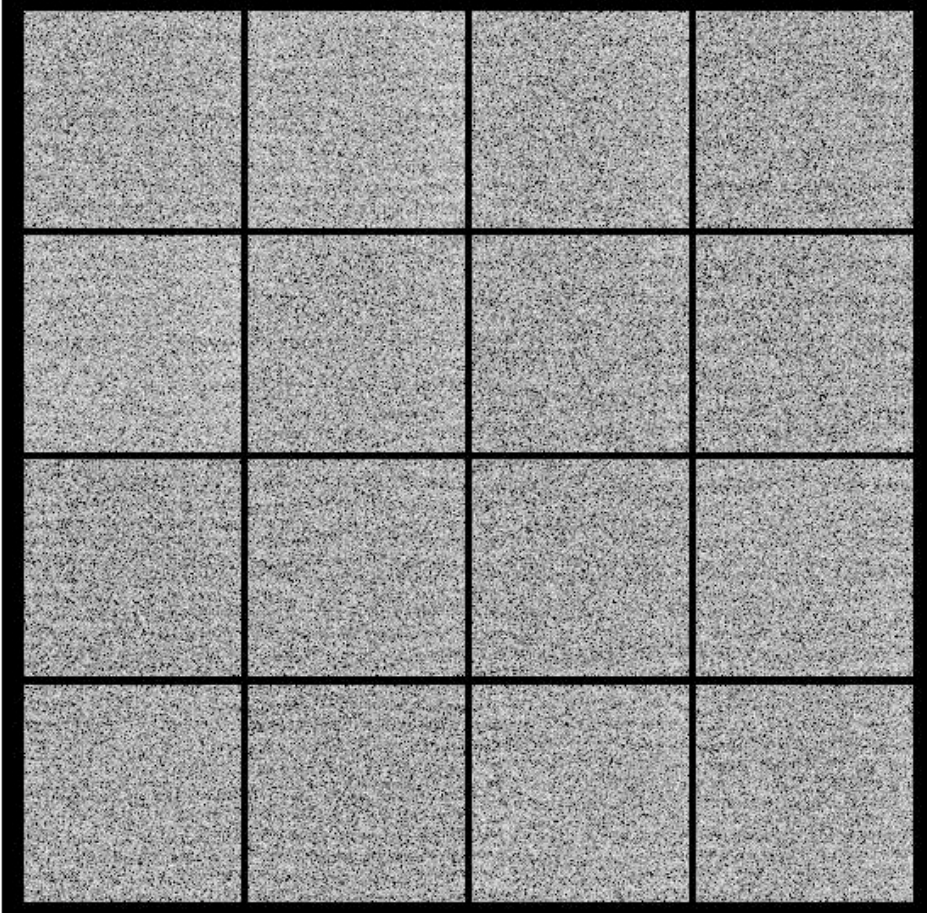


Figure 19. Zero-read difference images for 16 of the exposures in orbital test 3.

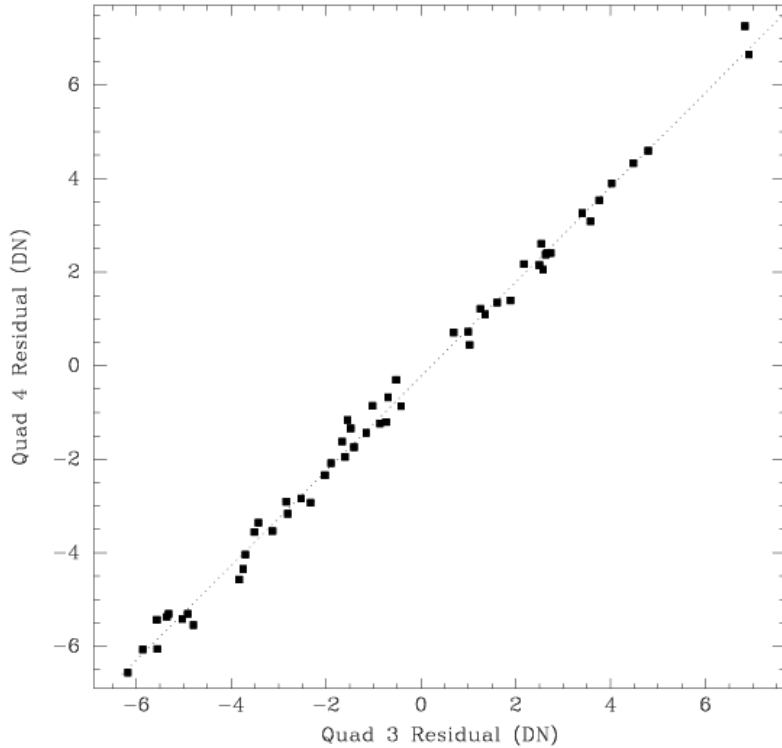


Figure 20. Mean residual signal in quadrants 3 and 4 for all of the zeroth-read difference images in orbital 3. The dotted line shows the fit to the data. There is a mean offset of 0.2 DN between these two quadrants, with an rms scatter of 0.25 DN about the fit.

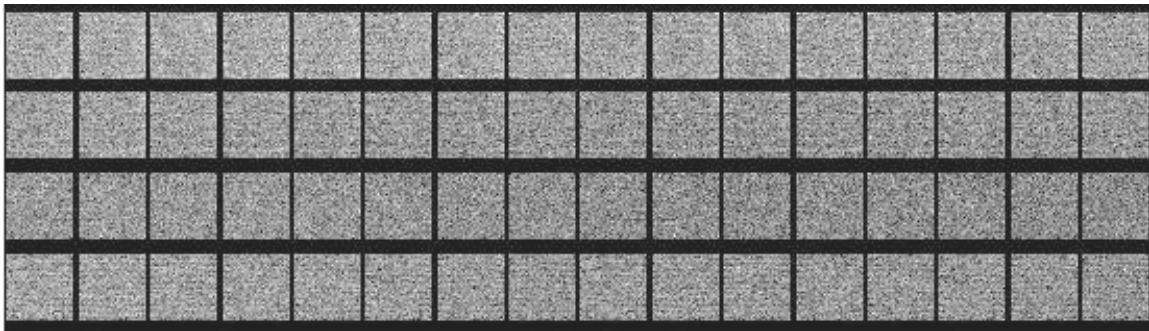


Figure 21. Read-by-read differences of 4 of the raw exposures in orbital test 3. The four different exposures are stacked top to bottom, with the 16 differences associated with the 16 readouts of each exposure displayed from left to right.

Conclusions

Variations in IR dark current resulting from the changing thermal and electrical environments during orbital cycling appear to be relatively small, amounting to a total difference in accumulated dark of ~ 5 e⁻/pixel in a 353 sec exposure, on average, or ~ 0.014 e⁻/sec/pix. Raw bias levels are correlated with WFC3 input power level, but the effect is complicated by an unexpected systematic variation in bias level from exposure

to exposure that appears to be dependent on exposure history – specifically the times when the detector is idling in flush mode. The changes in bias level track well across all image quadrants and the amplitude of the drifts is significantly reduced, but not completely eliminated, by the calibration process that uses the detector’s reference pixels to remove bias drifts. There is no indication of the type of quadrant-to-quadrant bias residuals seen in NICMOS images.

Acknowledgments

Thanks are due to the host of folks who tirelessly supported the TV3 campaign, as well as the WFC3 electrical engineers who were able to achieve this level of FPA temperature stability through their redesign and modifications of the IR TEC controller circuits.

References

Bergeron, L. E., 2005, The 2005 HST Calibration Workshop, “Temperature and Bias Variation and Measurement in the NICMOS Detectors”,
<http://www.stsci.edu/ts/webcasting/ppt/CalWorkshop2005/EddieBergeron102805A.ppt>

Hilbert, B., 2008, WFC3 ISR 2008-50, “WFC3 TV3 Testing: IR Gain Results.”

Appendix A: Image information for the orbital cycling tests.

Table 1. Image information for the exposures in test 1: Side 2, cold environment.

TVNUM	OPUS file name	TVSTART (UT)	PDU Voltage	IRFPATMP (C)
49205	ii240201r_08065204545	2008-03-05T20:38:42	26.05	-127.96
49206	ii240202r_08065205223	2008-03-05T20:45:20	26.05	-127.87
49207	ii240204r_08065205900	2008-03-05T20:51:58	26.05	-127.87
49208	ii240206r_08065210513	2008-03-05T20:58:35	26.05	-127.87
49209	ii240209r_08065211810	2008-03-05T21:11:07	31.47	-127.96
49210	ii24020ar_08065212448	2008-03-05T21:17:45	30.72	-127.96
49211	ii24020cr_08065213125	2008-03-05T21:24:23	30.72	-127.96
49212	ii24020er_08065213738	2008-03-05T21:31:00	30.72	-127.96
49213	ii24020hr_08065215035	2008-03-05T21:43:32	29.82	-127.96
49214	ii24020ir_08065215713	2008-03-05T21:50:10	28.76	-127.96
49215	ii24020kr_08065220349	2008-03-05T21:56:47	27.86	-127.87
49216	ii24020mr_08065221001	2008-03-05T22:03:23	27.26	-127.87
49217	ii24020pr_08065222259	2008-03-05T22:15:56	26.96	-127.87
49218	ii24020qr_08065222936	2008-03-05T22:22:33	28.91	-127.96
49219	ii24020sr_08065223614	2008-03-05T22:29:12	30.27	-127.96
49220	ii24020ur_08065224227	2008-03-05T22:35:49	30.72	-127.96
49221	ii24020xr_08065225524	2008-03-05T22:48:21	31.32	-127.96
49222	ii24020yr_08065230202	2008-03-05T22:54:59	31.47	-127.96
49223	ii240210r_08065230839	2008-03-05T23:01:37	31.32	-127.96
49224	ii240212r_08065231452	2008-03-05T23:08:14	31.17	-127.87
49225	ii240215r_08065232749	2008-03-05T23:20:46	30.72	-127.96
49226	ii240216r_08065233427	2008-03-05T23:27:24	29.67	-127.87
49227	ii240218r_08065234104	2008-03-05T23:34:02	28.76	-127.87
49228	ii24021ar_08065234717	2008-03-05T23:40:39	28.16	-127.87
49229	ii24021dr_08066000039	2008-03-05T23:53:12	27.11	-127.87

Table 2. Image information for the exposures in test 2: Side 1, cold environment.

TVNUM	OPUS file name	TVSTART (UT)	PDU Voltage	IRFPATMP (C)
49284	ii240201r_08066231344	2008-03-06T23:06:41	25.45	-128.71
49285	ii240202r_08066232022	2008-03-06T23:13:19	25.45	-128.71
49286	ii240204r_08066232659	2008-03-06T23:19:57	25.45	-128.71

WFC3 Instrument Science Report 2009-02

49287	ii240206r_08066233312	2008-03-06T23:26:34	25.45	-128.71
49288	ii240209r_08066234609	2008-03-06T23:39:06	31.47	-128.80
49289	ii24020ar_08066235247	2008-03-06T23:45:44	30.72	-128.71
49290	ii24020cr_08066235924	2008-03-06T23:52:22	30.72	-128.80
49291	ii24020er_08067000538	2008-03-06T23:59:00	30.87	-128.71
49292	ii24020hr_08067001835	2008-03-07T00:11:32	29.36	-128.71
49293	ii24020ir_08067002513	2008-03-07T00:18:10	28.46	-128.71
49294	ii24020kr_08067003150	2008-03-07T00:24:48	27.71	-128.80
49295	ii24020mr_08067003803	2008-03-07T00:31:25	27.26	-128.71
49296	ii24020pr_08067005100	2008-03-07T00:43:57	27.26	-128.71
49297	ii24020qr_08067005738	2008-03-07T00:50:35	28.76	-128.80
49298	ii24020sr_08067010415	2008-03-07T00:57:13	30.27	-128.71
49299	ii24020ur_08067011028	2008-03-07T01:03:50	30.57	-128.71
49300	ii24020xr_08067012325	2008-03-07T01:16:22	30.72	-128.71
49301	ii24020yr_08067013003	2008-03-07T01:23:00	31.47	-128.71
49302	ii240210r_08067013640	2008-03-07T01:29:38	30.72	-128.80
49303	ii240212r_08067014253	2008-03-07T01:36:15	30.87	-128.71
49304	ii240215r_08067015550	2008-03-07T01:48:47	30.57	-128.71
49305	ii240216r_08067020228	2008-03-07T01:55:25	29.67	-128.71
49306	ii240218r_08067020905	2008-03-07T02:02:03	28.76	-128.71
49307	ii24021ar_08067021518	2008-03-07T02:08:40	27.71	-128.80
49308	ii24021dr_08067022815	2008-03-07T02:21:12	26.50	-128.71
49309	ii24021er_08067023453	2008-03-07T02:27:50	26.80	-128.71
49310	ii24021gr_08067024130	2008-03-07T02:34:28	28.91	-128.80
49311	ii24021ir_08067024743	2008-03-07T02:41:05	30.12	-128.80
49312	ii24021lr_08067030040	2008-03-07T02:53:37	30.87	-128.80
49313	ii24021mr_08067030718	2008-03-07T03:00:15	31.02	-128.71
49314	ii24021or_08067031355	2008-03-07T03:06:53	31.32	-128.80
49315	ii24021qr_08067032008	2008-03-07T03:13:30	31.47	-128.80
49316	ii24021tr_08067033305	2008-03-07T03:26:02	30.72	-128.71
49317	ii24021ur_08067033943	2008-03-07T03:32:40	30.57	-128.71
49318	ii24021wr_08067034620	2008-03-07T03:39:18	29.67	-128.80
49319	ii24021yr_08067035233	2008-03-07T03:45:55	28.61	-128.71
49320	ii240221r_08067040530	2008-03-07T03:58:27	27.71	-128.71
49321	ii240222r_08067041208	2008-03-07T04:05:05	26.96	-128.71
49322	ii240224r_08067041845	2008-03-07T04:11:43	26.05	-128.80
49323	ii240226r_08067042547	2008-03-07T04:18:20	28.31	-128.71

Table 3. Image information for the exposures in test 3: Side 1, hot environment.

TVNUM	OPUS file name	TVSTART (UT)	PDU Voltage	IRFPATMP (C)
52728	ii240201r_08080121544	2008-03-20T12:08:41	31.47	-128.80
52729	ii240202r_08080122222	2008-03-20T12:15:19	31.47	-128.71
52730	ii240204r_08080122859	2008-03-20T12:21:57	31.47	-128.71
52731	ii240206r_08080123512	2008-03-20T12:28:34	31.47	-128.71
52732	ii240209r_08080124809	2008-03-20T12:41:06	31.47	-128.80
52733	ii24020ar_08080125447	2008-03-20T12:47:44	31.47	-128.80
52734	ii24020cr_08080130124	2008-03-20T12:54:22	31.17	-128.71
52735	ii24020er_08080130737	2008-03-20T13:00:59	31.47	-128.71
52736	ii24020hr_08080132034	2008-03-20T13:13:31	31.47	-128.71
52737	ii24020ir_08080132712	2008-03-20T13:20:09	31.47	-128.71
52738	ii24020kr_08080133349	2008-03-20T13:26:47	31.17	-128.80
52739	ii24020mr_08080134002	2008-03-20T13:33:24	31.17	-128.71
52740	ii24020pr_08080135259	2008-03-20T13:45:56	31.17	-128.71
52741	ii24020qr_08080135937	2008-03-20T13:52:34	31.47	-128.71
52742	ii24020sr_08080140614	2008-03-20T13:59:12	31.47	-128.71
52743	ii24020ur_08080141227	2008-03-20T14:05:49	31.47	-128.80
52744	ii240201r_08080142944	2008-03-20T14:22:41	31.47	-128.80
52745	ii240202r_08080143622	2008-03-20T14:29:19	31.47	-128.71
52746	ii240204r_08080144259	2008-03-20T14:35:57	31.17	-128.71
52747	ii240206r_08080144912	2008-03-20T14:42:34	30.72	-128.80
52748	ii240209r_08080150209	2008-03-20T14:55:06	30.12	-128.71
52749	ii24020ar_08080150847	2008-03-20T15:01:44	28.76	-128.71
52750	ii24020cr_08080151524	2008-03-20T15:08:22	27.86	-128.71
52751	ii24020er_08080152137	2008-03-20T15:14:59	27.71	-128.71
52752	ii24020hr_08080153434	2008-03-20T15:27:31	25.90	-128.71
52753	ii24020ir_08080154112	2008-03-20T15:34:09	28.31	-128.71
52754	ii24020kr_08080154749	2008-03-20T15:40:47	29.97	-128.71
52755	ii24020mr_08080155402	2008-03-20T15:47:24	30.57	-128.80
52756	ii24020pr_08080160659	2008-03-20T15:59:56	30.87	-128.71
52757	ii24020qr_08080161337	2008-03-20T16:06:34	31.47	-128.80
52758	ii24020sr_08080162014	2008-03-20T16:13:12	31.17	-128.80
52759	ii24020ur_08080162627	2008-03-20T16:19:49	30.87	-128.71
52760	ii24020xr_08080163924	2008-03-20T16:32:21	30.72	-128.71
52761	ii24020yr_08080164602	2008-03-20T16:38:59	30.27	-128.71
52762	ii240210r_08080165239	2008-03-20T16:45:37	28.76	-128.71
52763	ii240212r_08080165852	2008-03-20T16:52:14	28.46	-128.71

WFC3 Instrument Science Report 2009-02

52764	ii240215r_08080171149	2008-03-20T17:04:46	26.96	-128.71
52765	ii240216r_08080171827	2008-03-20T17:11:24	26.35	-128.71
52766	ii240218r_08080172504	2008-03-20T17:18:02	27.71	-128.80
52767	ii24021ar_08080173117	2008-03-20T17:24:39	29.67	-128.80
52768	ii24021dr_08080174414	2008-03-20T17:37:11	30.72	-128.80
52769	ii24021er_08080175052	2008-03-20T17:43:49	31.17	-128.80
52770	ii24021gr_08080175729	2008-03-20T17:50:27	31.47	-128.71
52771	ii24021ir_08080180342	2008-03-20T17:57:04	31.17	-128.71
52772	ii24021lr_08080181639	2008-03-20T18:09:36	30.72	-128.71
52773	ii24021mr_08080182317	2008-03-20T18:16:14	31.17	-128.71
52774	ii24021or_08080182954	2008-03-20T18:22:52	30.57	-128.71
52775	ii24021qr_08080183607	2008-03-20T18:29:29	28.91	-128.71
52776	ii24021tr_08080184904	2008-03-20T18:42:01	27.71	-128.71
52777	ii24021ur_08080185542	2008-03-20T18:48:39	27.26	-128.71
52778	ii24021wr_08080190219	2008-03-20T18:55:17	26.20	-128.71
52779	ii24021yr_08080190832	2008-03-20T19:01:54	27.56	-128.71
52780	ii240221r_08080192129	2008-03-20T19:14:26	30.42	-128.71
52781	ii240222r_08080192807	2008-03-20T19:21:04	30.72	-128.71
52782	ii240224r_08080193444	2008-03-20T19:27:42	30.72	-128.80
52783	ii240226r_08080194146	2008-03-20T19:34:19	30.87	-128.71